

This is the accepted manuscript made available via CHORUS. The article has been published as:

# Optimization of the figure of merit in $\text{Bi}_{100-x}\text{Sb}_x/\text{Al}_2\text{O}_3$ nanocomposites

Hyungyu Jin and Joseph P. Heremans

Phys. Rev. Materials **2**, 115401 — Published 26 November 2018

DOI: [10.1103/PhysRevMaterials.2.115401](https://doi.org/10.1103/PhysRevMaterials.2.115401)

# Optimization of the Figure-of-Merit in Bi-Sb/Al<sub>2</sub>O<sub>3</sub> Nanocomposites

Hyungyu Jin<sup>1\*</sup> and Joseph P. Heremans<sup>2,3,4</sup>

1. Department of Mechanical Engineering, Pohang University of Science and Technology (POSTECH), Pohang 37673, South Korea
2. Department of Mechanical and Aerospace Engineering, The Ohio State University, Columbus, OH, 43210
3. Department of Materials Science and Engineering, The Ohio State University, Columbus, OH, 43210
4. Department of Physics, The Ohio State University, Columbus, OH, 43210

\*Email address: [hgjin@postech.ac.kr](mailto:hgjin@postech.ac.kr)

## ABSTRACT

Bismuth-antimony (Bi<sub>100-x</sub>Sb<sub>x</sub>) alloys have the highest thermoelectric figure of merit of all n-type thermoelectric materials below 200 K. They are the only Te-free thermoelectric alternatives to the tetradymite materials for applications at and below room temperature. Single-crystal Bi<sub>100-x</sub>Sb<sub>x</sub> alloys show the maximum figure-of-merit  $zT \sim 0.5$  at 200K along the trigonal axis crystallographic direction, but the cost associated with single-crystal growth and the tendency of single crystals to cleave preclude their use. Mechanically robust polycrystalline Bi<sub>100-x</sub>Sb<sub>x</sub>/Al<sub>2</sub>O<sub>3</sub> nanocomposites are shown here to be able to reach competitive  $zT$  values. Two compositions are investigated, Bi<sub>82</sub>Sb<sub>18</sub> and Bi<sub>88</sub>Sb<sub>12</sub>. Thermal and electrical transport properties confirm significant reduction of lattice thermal conductivity in the nanocomposite samples, but the concurrent loss of electrical conductivity leads to unfavorable net effect on  $zT$ . In contrast, a large increase in thermopower is observed in the Bi<sub>82</sub>Sb<sub>18</sub>/Al<sub>2</sub>O<sub>3</sub> nanocomposite system, which is attributed to better optimized doping level. Accordingly, the  $zT$  of a Bi<sub>82</sub>Sb<sub>18</sub>/Al<sub>2</sub>O<sub>3</sub> nanocomposite sample is shown to reach  $zT \sim 0.4$  at 240 K, which rivals that of single crystals. Near room temperature, the  $zT$  of the nanocomposite sample is improved by  $\sim 60\%$  over that of the single crystalline sample. Galvano- and thermo-magnetic analysis suggests a strong effect of carrier concentration on the  $zT$  of Bi-Sb/Al<sub>2</sub>O<sub>3</sub> nanocomposite samples.

## INTRODUCTION

Bismuth-antimony ( $\text{Bi}_{100-x}\text{Sb}_x$ ) alloys have the highest  $zT$  of all n-type thermoelectric materials below about 200K.<sup>1</sup> Unlike elemental Bi, which is a semimetal with a band overlap<sup>2</sup>,  $\text{Bi}_{100-x}\text{Sb}_x$  alloys with  $7 < x < 20$  become narrow-gap semiconductors with a finite band gap whose size depends on  $x$ .<sup>3</sup> The semiconducting  $\text{Bi}_{100-x}\text{Sb}_x$  alloys show better thermoelectric performance compared to elemental Bi, because in elemental Bi, electron and hole partial thermopowers compensate each other, which leads to an overall thermopower that is smaller than in semiconductors with the same charge carrier concentration. Alloy scattering of phonons also lowers the lattice thermal conductivity of  $\text{Bi}_{100-x}\text{Sb}_x$  alloys compared to that of elemental Bi. Finally, unlike the commercial tetradymite  $(\text{Bi}_{100-x}\text{Sb}_x)_2(\text{Te}_{100-y}\text{Se}_y)_3$  alloys<sup>4</sup> that dominate the thermoelectric industry,  $\text{Bi}_{100-x}\text{Sb}_x$  alloys contain no Te, an element that is rare in the Earth's crust. In cost-sensitive thermoelectric applications, the Peltier elements sometimes are cut so small that the effective Peltier-module figure-of-merit or  $ZT$  (typically 0.4 to 0.7) is greatly reduced compared to the material  $zT$  (typically 0.9 to 1.2). Here, the material has a  $zT \equiv \left( \frac{S^2 \sigma}{\kappa} \right) T$ , where  $S$  is the Seebeck coefficient or thermopower,  $\sigma$  the electrical conductivity,  $\kappa$  the thermal conductivity, and  $T$  the temperature. Under those circumstances, using larger  $\text{Bi}_{100-x}\text{Sb}_x$  elements at a lower material cost may be competitive with smaller  $(\text{Bi}_{100-x}\text{Sb}_x)_2(\text{Te}_{100-y}\text{Se}_y)_3$  elements producing the same net device  $ZT$ . Unfortunately, values of  $zT \geq 0.4$  until now have been achieved only in single-crystal  $\text{Bi}_{100-x}\text{Sb}_x$  ( $x < 20$  at. %) alloys along the trigonal axis direction normal to the cleavage plane, raising unsurmountable mechanical problems in Peltier coolers.

While extensive studies have been done on thermoelectric properties of single-crystalline  $\text{Bi}_{100-x}\text{Sb}_x$  alloys<sup>5,6,7,8,9</sup> as well as polycrystalline samples<sup>10,11,12,13</sup>, almost no noticeable improvement has been achieved in  $zT$  of these alloys, still limited to a maximum  $zT$  of  $\sim 0.5$  at 200K for single crystalline samples.

Due to strong anisotropy, single crystalline  $\text{Bi}_{100-x}\text{Sb}_x$  alloys possess much better thermoelectric performance along the trigonal axis direction, compared to that in the trigonal plane direction consisting of binary and bisectrix axes. The room temperature  $zT$  of single crystalline  $\text{Bi}_{100-x}\text{Sb}_x$  alloys for different  $x$  values as reported by Yim and Amith<sup>5</sup> is shown in **Fig. 1**. The  $zT$  is maximum around  $x = 12$  at. % in both trigonal axis and binary/bisectrix axis (trigonal plane) directions, but the anisotropy decreases markedly above  $x = 15$  at. %. These single crystalline alloys cleave easily along the trigonal plane direction, which presents mechanical stability issues for practical applications, as mentioned above. Polycrystalline  $\text{Bi}_{100-x}\text{Sb}_x$  alloys, on the other hand, comprise small crystals with random orientations, which make them more robust against mechanical stress and have thermoelectric performance somewhere between that of trigonal axis and trigonal plane directions. To estimate the  $zT$  of polycrystalline  $\text{Bi}_{100-x}\text{Sb}_x$  alloys for different  $x$  values, **Fig. 1** also shows the average of the single crystal data, and the results show good agreement with the experimental results by Lenoir et al<sup>11</sup>. The average has a broad maximum centered around  $x = 12$  at. % ; the present study therefore is focused on this concentration and also on  $x = 18$  at. % for comparison.

It has been shown<sup>14,15,16,17</sup> that under circumstances where the electron mean free path is much shorter than the phonon mean free path, nanostructuring can effectively reduce the lattice thermal conductivity of thermoelectric materials while not affecting  $S$  and  $\sigma$  that much, thus leading to improvement of  $zT$ . Although proven effective, nanostructuring has fundamental limitations in practical applications due to grain growth during thermal cycles at temperatures near the melting point. Besides the thermal conductivity reduction, nanostructuring was also suggested as a way to induce the size quantization effect proposed by Hicks and Dresselhaus<sup>18,19</sup>. Hicks and Dresselhaus theoretically predicted that the size quantization effect in a low dimensional system can induce a sharp increase in the local density of states, which in turn can be utilized to enhance  $S$  of thermoelectric materials. The concept was experimentally demonstrated by Heremans *et al.*<sup>20</sup> on Bi nanowires embedded in porous host materials, for which  $S$

increased orders of magnitude due to the size quantization effect. Unfortunately, at the time those results were produced, it proved impossible to insert a large enough volume fraction of Bi in the host material, so that the increase in electrical resistivity due to size-quantization was not overcome by a corresponding decrease in thermal conductivity, as the overall thermal conductance was dominated by the porous host material<sup>21</sup>.

Here we investigate the effect of nanostructuring in  $\text{Bi}_{100-x}\text{Sb}_x$  alloys by synthesizing  $\text{Bi}_{100-x}\text{Sb}_x/\text{Al}_2\text{O}_3$  nanocomposites ( $x = 12$  and  $18$  at. %). By utilizing the ball-milling technique, we were able to synthesize bulk nanocomposite samples, thus avoiding the fill fraction issue in the previous study<sup>20</sup>. We introduced  $\text{Al}_2\text{O}_3$  nanoparticles (diameter = 40 to 50 nm) with varying volume percentages in  $\text{Bi}_{100-x}\text{Sb}_x$  host matrices, effectively creating nanocomposites with well-dispersed nanoscale inclusions. We present experimental results of thermal and electrical transport in the  $\text{Bi}_{100-x}\text{Sb}_x/\text{Al}_2\text{O}_3$  samples, and show that  $zT$  reaches near 0.4 at 240 K. We discuss the results with regard to carrier scattering and carrier concentration, based on rigorous galvanic- and thermo-magnetic analyses.

## EXPERIMENTAL

### Sample preparation

The appropriate amounts of 6N-pure Alfa-Aesar Bi and Sb were coarsely ground with mortar and pestle in a glove-box, and introduced into a stainless-steel ball-milling vessel. The appropriate amount of Alfa-Aesar NanoTek  $\text{Al}_2\text{O}_3$  powder, with 40-50 nm diameter particles, was added to the vessel. The vessel was sealed within a glove-box, extracted from it, and the content was milled for 80 minutes in a SPEX 8000M high energy ball-mill. Materials were mixed and ground in stainless steel vials with two ½” and

four ¼” stainless steel balls. After this, the vessel was re-introduced into the glove box, opened, and the powder was transferred into a graphite die. The powder was pressed using a 3 ton hydraulic press. The pressed pellets were introduced into a quartz ampoule, which was evacuated and sealed at less than  $10^{-6}$  Torr, and the material was subsequently sintered at 265 °C for 150 hours. The mass density of the samples was measured using the Archimedes method. All of the nanocomposite samples with  $\text{Al}_2\text{O}_3$  show the quite consistent mass density of ~92 % relative to their theoretical values, while the samples without  $\text{Al}_2\text{O}_3$  have ~93 %. Samples were then cut into approximately  $2 \times 1 \times 7 \text{ mm}^3$  parallelepipeds, and their thermoelectric, thermomagnetic, and galvanomagnetic properties were measured at temperatures from 80 K to 420 K and with magnetic field up to 1.4 T using a custom liquid nitrogen cryostat system.

Scanning electron microscopy (SEM) pictures for the  $\text{Bi}_{82}\text{Sb}_{18}/\text{Al}_2\text{O}_3$  nanocomposite samples with 5 and 20 vol. %  $\text{Al}_2\text{O}_3$  nanoparticles are shown in **Fig. 2**. While fairly well distributed  $\text{Al}_2\text{O}_3$  nanoparticles are observed, it is not clear whether effective nanoscale channels are formed in the samples. Seemingly, 5 vol. % of  $\text{Al}_2\text{O}_3$  is too scarce to form such channels.

### **$\text{Bi}_{82}\text{Sb}_{18}/\text{Al}_2\text{O}_3$ nanocomposites**

**Figure 3** shows the thermoelectric properties of  $\text{Bi}_{82}\text{Sb}_{18}/\text{Al}_2\text{O}_3$  nanocomposite samples with 0, 5 and 20 vol. %  $\text{Al}_2\text{O}_3$ . We compare the data to calculated values for the thermoelectric properties of the single crystalline  $\text{Bi}_{82}\text{Sb}_{18}$  sample in Ref. [5], by taking a weighted average of the data along the three crystallographic directions.  $\kappa(T)$  of the nanocomposite samples shown in **Fig. 3(a)** are significantly reduced compared to that of the single crystalline sample and decreases as the volume percentage of  $\text{Al}_2\text{O}_3$  increases. It is possible to estimate how much reduction in  $\kappa(T)$  comes from each of electronic and lattice contributions by measuring the magnetic field dependence of the thermal conductivity,  $\kappa(H)$  where  $H$  is the external

magnetic field applied in the transverse direction. The inset in **Fig. 3(a)** shows  $\kappa(H)$  normalized by the zero-field value,  $\kappa(H) / \kappa(H=0)$  at  $T = 100$  K. The  $\kappa(H) / \kappa(H=0)$  of the  $\text{Bi}_{82}\text{Sb}_{18}/\text{no Al}_2\text{O}_3$  sample decreases with increasing  $H$ , and saturates at  $H > 1.0$  T. This saturation indicates complete suppression of the electronic contribution to  $\kappa$ , leaving only the lattice contribution<sup>22,23</sup>. The electronic contribution in the  $\text{Bi}_{82}\text{Sb}_{18}/\text{no Al}_2\text{O}_3$  is estimated to be 17 % of the total  $\kappa$ . By repeating the same procedure for the two  $\text{Bi}_{82}\text{Sb}_{18}$  nanocomposite samples, we obtain the electronic contribution of 8 % and 5 % for the 5 vol. % and 20 vol. %  $\text{Al}_2\text{O}_3$  samples, respectively. The difference in those values between the no  $\text{Al}_2\text{O}_3$  sample and the nanocomposite samples accounts for the amount of reduction in the electronic contribution due to the presence of  $\text{Al}_2\text{O}_3$  nanoparticles – 9 % and 12 % for the 5 vol. % and 20 vol. %  $\text{Al}_2\text{O}_3$  samples, respectively. The rest 91% and 88 % reductions come from the lattice contribution. Therefore, the reduction in  $\kappa(T)$  in the  $\text{Bi}_{82}\text{Sb}_{18}/\text{Al}_2\text{O}_3$  samples is mainly attributed to the reduction of the lattice thermal conductivity due to phonon scattering by the  $\text{Al}_2\text{O}_3$  nanoparticles and grain boundaries in the polycrystalline samples. On the other hand, the electrical resistivity ( $\rho = 1/\sigma$ ) shown in **Fig. 3(b)** shows a large increase over the measurement temperature regime as the  $\text{Al}_2\text{O}_3$  content increases. The carrier concentration ( $n$ ) data obtained from Hall coefficient ( $R_H$ ) measurements, shown in **Fig. 4(a)**, show that the addition of the  $\text{Al}_2\text{O}_3$  slightly reduces  $n$ , but not so much to account for the increase in  $\rho(T)$ . The Hall mobility ( $\mu_H$ ) data, shown in **Fig. 4(b)**, suggest that the  $\text{Al}_2\text{O}_3$  nanoparticles also strongly scatter conduction electrons. The ratios of the  $\rho(T)$  of the materials for  $\text{Al}_2\text{O}_3$  loadings of 0, 5 and 20% are 1:3:9 at 300 K. The thermal resistivity, the inverse of the  $\kappa$ , increases in ratios of 1:2:6 at the same temperature. We conclude that the  $\text{Al}_2\text{O}_3$  nanoparticles scatter electrons more than they scatter phonons, and that the ratio between the electrical and thermal conductivities is thus slightly unfavorable to  $zT$ . Sharp and Goldsmid theoretically studied the effect of grain boundary scattering on  $zT$  of SiGe, Bi-Sb, and  $\text{Bi}_2\text{Te}_3$  alloys<sup>24,25,26</sup>. They concluded that while grain boundary scattering can significantly enhance the  $zT$  of SiGe alloys down to a certain grain size, it is

unlikely to be useful for Bi-Sb and Bi<sub>2</sub>Te<sub>3</sub> alloys wherein conduction electrons with long mean free paths are scattered much more than phonons by small grain boundaries. Their prediction is consistent with what we observe in the Bi<sub>82</sub>Sb<sub>18</sub>/Al<sub>2</sub>O<sub>3</sub> nanocomposite samples.

In contrast,  $S(T)$  is very favorably influenced by the presence of Al<sub>2</sub>O<sub>3</sub> nanoparticles (**Fig. 3(c)**). The concentration of those particles has little effect, but their presence increases the absolute value of  $S(T)$  by 25% near room temperature. This increase more than compensates the loss mentioned in the previous paragraph, so that the  $zT$  of the Bi<sub>82</sub>Sb<sub>18</sub> / 5% Al<sub>2</sub>O<sub>3</sub> sample is improved above 180 K compared to that of the sample with no Al<sub>2</sub>O<sub>3</sub> and reaches its maximum value  $\sim 0.4$  at 240 K as shown in **Fig. 3(d)**. It also is noted that the peak  $zT$  is shifted to higher temperatures for the nanocomposite samples. Since the origin of the improvement lies in the enhanced  $S(T)$ , we can speculate about the physical mechanisms that can give rise to the effect. The first possibility is the size-quantization effect in some channels of Bi<sub>82</sub>Sb<sub>18</sub> alloys that might exist in-between the Al<sub>2</sub>O<sub>3</sub> nanoparticles. We exclude this possibility based on the SEM results (**Fig. 2**) as well as on the fact that no noticeable increase in the electron effective mass has been observed in the nanocomposite samples as described below.

A second possibility is an increase in the energy dependence of the relaxation time. Such a mechanism was proven to be the physical origin of a similar observation made in nanostructured PbTe<sup>14</sup> prepared in a similar way. Here as well, we explore such possibility by analyzing the thermomagnetic and galvanomagnetic properties. The magnetic field dependence of the Nernst voltage (not shown) becomes very non-linear above 120 K, and shows the opposite sign between the low-field ( $\mu H \ll 1$ , where  $\mu$  is the electron mobility and  $H$  is the applied magnetic field) and the high-field ( $\mu H > 1$ ). Here we only consider the low-field ( $\mu H \ll 1$ ) Nernst coefficient ( $N$ ) in our analysis where the Nernst voltage is linear in  $H$ . The temperature dependence of the low-field  $N$  (**Fig. 4(c)**) shows a sharp contrast in its behavior between the



samples with and without Al<sub>2</sub>O<sub>3</sub> nanoparticles, indicating that different scattering mechanisms dominate in the two systems. While the low-field  $N$  of the samples with Al<sub>2</sub>O<sub>3</sub> nanoparticles stays positive and is relatively small in the measured temperature range, that of the sample with no Al<sub>2</sub>O<sub>3</sub> shows a sign change from negative to positive below 180 K where it also features a strong temperature dependence; this is normal, since the  $N$  is particularly sensitive to the details of the scattering mechanism. The scattering mechanism changes enough with the introduction of Al<sub>2</sub>O<sub>3</sub> nanoparticles to affect the  $N$ , but not, as reported below, the  $S$ . Next, the “method of the four coefficients”<sup>14,27</sup> was applied to the Bi<sub>82</sub>Sb<sub>18</sub> data. In this method, one uses four transport coefficients, the resistivity ( $\rho = 1/\sigma$ ), Hall coefficient ( $R_H$ ), Nernst coefficient ( $N$ ) and thermopower ( $S$ ), to determine four transport parameters, the density-of-states effective mass ( $m_D^*$ ), Fermi energy ( $E_F$ ), mobility ( $\mu$ ) and scattering parameter ( $\lambda$ ). For non-parabolic and non-degenerate systems, the energy dependence of electron scattering is represented by that of the relaxation time as:<sup>27,28</sup>

$$\tau = \tau_0 \frac{\gamma(E)^\lambda}{\gamma'(E)}, \quad (1)$$

where  $\tau_0$  is an energy-independent scaling coefficient,  $\gamma(E) = E \left(1 + E/E_g\right)$  ( $E_g$  is the energy band gap),  $\gamma'$  is the derivative of  $\gamma$  with respect to  $E$ , and  $\lambda$  is the scattering parameter whose value depends on the scattering mechanism. Typically, for acoustic phonon scattering,  $\lambda = -0.5$  while for ionized impurity scattering,  $\lambda = 1.5$ , but in practice, given the error bars, one usually finds  $-0.8 < \lambda < 1.6$ . The electrical conductivity is:<sup>27</sup>

$$\sigma = \frac{(2m_D^* k_B T)^{3/2}}{3\pi^2 \hbar^3} \frac{e^2}{m_a^*} \int_0^\infty \frac{\gamma(z)^{3/2}}{\gamma'(z)} \tau(z) \left( -\frac{\partial f_0}{\partial z} \right) dz, \quad (2)$$

where  $e$  is the carrier charge,  $k_B$  is the Boltzmann constant,  $\hbar$  is the reduced Planck constant,  $m_\alpha^*$  is the effective mass along the crystallographic direction of the sample studied, or the appropriate average mass for polycrystals, and  $f_0$  is the Fermi-Dirac distribution function. The low-field ( $\mu H \ll 1$ ) Hall coefficient is:

$$R_H = \frac{3K(K+2)}{(2K+1)^2} \frac{1}{ne} \frac{\left\{ \int_0^\infty \frac{\gamma(z)^{3/2}}{(\gamma'(z))^2} \tau^2(z) \left( -\frac{\partial f_0}{\partial z} \right) dz \right\} \left\{ \int_0^\infty \gamma(z)^{3/2} \left( -\frac{\partial f_0}{\partial z} \right) dz \right\}}{\left\{ \int_0^\infty \frac{\gamma(z)^{3/2}}{\gamma'(z)} \tau(z) \left( -\frac{\partial f_0}{\partial z} \right) dz \right\}^2}, \quad (3)$$

where  $K$  is the effective mass anisotropy coefficient,  $K = m_l^*/m_t^*$  ( $m_l^*$  and  $m_t^*$  are the electron effective masses along the longitudinal and transverse directions, respectively). The low-field ( $\mu H \ll 1$ ) isothermal Nernst coefficient is:

$$N = R_H \sigma \frac{k_B}{e} \left\{ \frac{\int_0^\infty \frac{\gamma(z)^{3/2}}{(\gamma'(z))^2} z \tau^2(z) \left( -\frac{\partial f_0}{\partial z} \right) dz}{\int_0^\infty \frac{\gamma(z)^{3/2}}{(\gamma'(z))^2} \tau^2(z) \left( -\frac{\partial f_0}{\partial z} \right) dz} - \frac{\int_0^\infty \frac{\gamma(z)^{3/2}}{\gamma'(z)} z \tau(z) \left( -\frac{\partial f_0}{\partial z} \right) dz}{\int_0^\infty \frac{\gamma(z)^{3/2}}{\gamma'(z)} \tau(z) \left( -\frac{\partial f_0}{\partial z} \right) dz} \right\}, \quad (4)$$

and the thermopower is:

$$S = \frac{k_B}{e} \left\{ \frac{\int_0^\infty \frac{\gamma(z)^{3/2}}{\gamma'(z)} z \tau(z) \left( -\frac{\partial f_0}{\partial z} \right) dz}{\int_0^\infty \frac{\gamma(z)^{3/2}}{\gamma'(z)} \tau(z) \left( -\frac{\partial f_0}{\partial z} \right) dz} - \frac{E_F}{k_B T} \right\}. \quad (5)$$

For a degenerate semiconductor ( $E_F \gg k_B T$ ) with a parabolic band and a single type of carriers, the energy dependence of relaxation time is simplified as  $\tau(E) \propto E^\lambda$ , and Eqs. (2) – (5) are now written as:<sup>28</sup>

$$\sigma = ne\mu, \quad (6)$$

$$R_H = \frac{1}{ne}, \quad (7)$$

$$N = \frac{\pi^2}{3} \left( \frac{k_B}{e} \right) \frac{k_B T}{E_F} \lambda \mu, \quad (8)$$

$$S = \frac{2\pi^{2/3}}{3^{5/3}} \frac{k_B^2}{e\hbar^2} T \left( \frac{3}{2} + \lambda \right) \frac{m_D^*}{n^{2/3}}. \quad (9)$$

As outlined above, Eqs. (6) – (9) are solved at each temperature for four transport parameters,  $m_D^*$ ,  $E_F$ ,  $\mu$  and  $\lambda$ . By using the  $m_D^*$  and  $\lambda$  derived from the method of the four coefficients and the  $n$  derived from the Hall measurements, we can find the origin of enhancement of  $S$  in the  $\text{Bi}_{82}\text{Sb}_{18}/\text{Al}_2\text{O}_3$  nanocomposite samples. **Figure 4(d)** shows that  $(3/2 + \lambda) \cdot m_D^*$  does not have strong dependence either on the  $\text{Al}_2\text{O}_3$  content or on temperature, all of the data points scattered within  $(0.18 \pm 0.03)$ . This observation suggests that the enhanced  $S$  of the nanocomposite samples actually originates from their lower  $n$ , not from either increased  $m_D^*$  or  $\lambda$ . Jandl and Birkholz<sup>29</sup> also showed that slight p-type doping by tin could increase the n-type  $S$  value in  $\text{Bi}_{95}\text{Sb}_5$  single crystals, thus leading to enhanced  $zT$  values above 200 K, which is consistent with our observation. Thus, we suggest that the lower  $S$  of both the sample with no  $\text{Al}_2\text{O}_3$  and the single crystalline sample from Ref. [5] is due to less optimally doped samples with larger  $n$ . Defects are known to alter the carrier concentration in Bi,<sup>30</sup> so that it is likely that the presence of  $\text{Al}_2\text{O}_3$  nanoparticles affects it as well. Vecchi et al.<sup>31</sup> reported the temperature dependence of the band gap between the conduction and valence bands at L-point for  $\text{Bi}_{100-x}\text{Sb}_x$  ( $0 \leq x \leq 15$ ) alloys, and showed that the band gap closes and band inversion happens near 180 K. Since we use the model for degenerate semiconductors based on a single type of carriers, we limit our analysis to the temperature range below 140 K where the thermal excitation is

relatively less significant. It is also noted that the L-point conduction band in Bi-Sb alloys is known to be non-parabolic. While this non-parabolicity could also introduce errors in estimating the values of the transport parameters, we find that the temperature-independent trend of  $(3/2 + \lambda) \cdot m_D^*$  remains consistent.

### **Bi<sub>88</sub>Sb<sub>12</sub>/Al<sub>2</sub>O<sub>3</sub> nanocomposites**

The thermoelectric properties of Bi<sub>88</sub>Sb<sub>12</sub>/Al<sub>2</sub>O<sub>3</sub> nanocomposite samples with 0, 5, 20, and 40 vol. % Al<sub>2</sub>O<sub>3</sub> are shown in **Fig. 5**, compared with those of a single crystalline Bi<sub>88</sub>Sb<sub>12</sub> sample calculated using the data from Ref. [5].  $\kappa(T)$  of the polycrystalline Bi<sub>88</sub>Sb<sub>12</sub> sample is slightly lower than that of the single crystalline sample, possibly due to its lower density as well as additional phonon scattering by grain boundary and defects. Introducing Al<sub>2</sub>O<sub>3</sub> nanoparticles significantly reduces  $\kappa(T)$ , suggesting that the 40 - 50 nm nanoparticles effectively scatter phonons.  $\rho(T)$  of the polycrystalline samples are considerably higher than that of the single crystalline samples, and rapidly increases as the Al<sub>2</sub>O<sub>3</sub> content increases. It is noted that the difference in  $\rho(T)$  between the polycrystalline Bi<sub>88</sub>Sb<sub>12</sub> sample and the single crystalline sample is larger than that in  $\kappa(T)$  between the two samples. Additionally, the rate at which  $\rho(T)$  increases with increasing Al<sub>2</sub>O<sub>3</sub> content is much larger than the rate at which  $\kappa(T)$  decreases. **Figure 6(b)** confirms that one of the mechanisms at work to increase  $\rho(T)$  is indeed scattering of conduction electrons by Al<sub>2</sub>O<sub>3</sub> nanoparticles. This conclusion is in line with the case of Bi<sub>82</sub>Sb<sub>18</sub>/Al<sub>2</sub>O<sub>3</sub> nanocomposite samples. The consistent results from the two different sample sets indicate that the Al<sub>2</sub>O<sub>3</sub> nanoparticles, small grain boundaries, and defects in the Bi<sub>100-x</sub>Sb<sub>x</sub> polycrystalline samples scatter phonons and electrons simultaneously, with more effect on the latter, thus unfavorably affecting  $zT$  values.

$S(T)$  of the polycrystalline samples shows enhancement compared to that of the single crystal, consistent with the case of  $\text{Bi}_{82}\text{Sb}_{18}$  samples. The behavior around and below 100 K of the polycrystalline  $\text{Bi}_{88}\text{Sb}_{12}$  sample containing no  $\text{Al}_2\text{O}_3$  is indicative of a classical narrow-gap semiconductor which shows carrier freeze-out. All samples containing  $\text{Al}_2\text{O}_3$  have a similar  $S(T)$ , but their curves never reach the high  $S(T)$  value of the polycrystalline  $\text{Bi}_{88}\text{Sb}_{12}$  sample with no  $\text{Al}_2\text{O}_3$  at 100 K. Overall,  $zT$  of the polycrystalline  $\text{Bi}_{88}\text{Sb}_{12}$  samples is inferior to that of the single crystalline sample over the measured temperature range, contrary to the case of  $\text{Bi}_{82}\text{Sb}_{18}$  samples. This is again due to the significantly reduced  $\sigma/\kappa$  ratio, which in this case is not compensated by the amount of increase in  $S(T)$ . Introducing  $\text{Al}_2\text{O}_3$  nanoparticles further reduces  $zT$  in the  $\text{Bi}_{88}\text{Sb}_{12}/\text{Al}_2\text{O}_3$  samples, because the presence of the  $\text{Al}_2\text{O}_3$  nanoparticles further deteriorates the  $\sigma/\kappa$  ratio while it affects  $S(T)$  little. This result is also in contrast to that of the  $\text{Bi}_{82}\text{Sb}_{18}/\text{Al}_2\text{O}_3$  samples, where the samples with  $\text{Al}_2\text{O}_3$  nanoparticles show better  $zT$  above 180 K. The discrepancy between the two systems is mainly attributed to the degree of optimal doping of the samples. While the  $\text{Bi}_{88}\text{Sb}_{12}/\text{Al}_2\text{O}_3$  samples also exhibit weak dependence of  $(3/2 + \lambda) \cdot m_D^*$  on the  $\text{Al}_2\text{O}_3$  content (**Fig. 6(d)**), there is almost no difference in  $n$  between the samples with and without  $\text{Al}_2\text{O}_3$  nanoparticles (**Fig. 6(a)**). Combined together, this leads to the fairly consistent  $S(T)$  between those samples, thus making their  $zT$  dependent mostly on the  $\sigma/\kappa$  ratio. As we have discussed earlier, the  $\text{Bi}_{82}\text{Sb}_{18}/\text{Al}_2\text{O}_3$  samples, on the other hand, have quite different  $n$  between the samples with and without  $\text{Al}_2\text{O}_3$  nanoparticles: the samples with  $\text{Al}_2\text{O}_3$  nanoparticles have smaller  $n$ , which yields the improved  $zT$  above 180 K compared to the sample without the nanoparticles. Therefore, we can conclude that in  $\text{Bi}_{100-x}\text{Sb}_x$  alloys ( $x = 12$  and  $18$  at. %), introduction of nanoscale inclusions unfavorably affects the  $\sigma/\kappa$  ratio as predicted by Sharp and Goldsmid<sup>24,25,26</sup>, while it barely affects  $S$  through altering the value of  $(3/2 + \lambda) \cdot m_D^*$ . It is noted,

nevertheless, that the  $zT$  of the nanocomposite samples can still be improved over that of the single crystalline sample by carefully adjusting  $n$  and thus enhancing  $S$  as in the case of  $\text{Bi}_{82}\text{Sb}_{18}/\text{Al}_2\text{O}_3$  samples.

## CONCLUSIONS

In summary, we present the experimental study of thermoelectric properties of  $\text{Bi}_{100-x}\text{Sb}_x/\text{Al}_2\text{O}_3$  nanocomposites ( $x = 12$  and  $18$  at. %), wherein we intentionally introduced various volume percentages of  $\text{Al}_2\text{O}_3$  nanoparticles with a goal of creating nanoscale channels in the  $\text{Bi}_{100-x}\text{Sb}_x$  matrix that could possibly increase the Seebeck coefficient either by size quantization effects or by enhanced scattering parameter. No proof was found of either effect in this study. The  $\text{Al}_2\text{O}_3$  nanoparticles may scatter phonons leading to the reduction of the lattice thermal conductivity. While such reduction of the lattice thermal conductivity is experimentally confirmed, it is found that the  $\text{Al}_2\text{O}_3$  nanoparticles also strongly scatter conduction electrons, resulting in unfavorable net effect on the electrical to thermal conductivity ratio. On the other hand, the enhancement of the Seebeck coefficient in the  $\text{Bi}_{82}\text{Sb}_{18}/\text{Al}_2\text{O}_3$  nanocomposite samples is large enough to compensate the loss due to scattering of conduction electrons, which overall leads to an improved figure-of-merit above  $180$  K compared to that of a single crystalline counterpart as well as the sample with no  $\text{Al}_2\text{O}_3$ . The peak figure-of-merit is shifted to higher temperatures for the nanocomposite samples, reaching the value of  $\sim 0.4$  at  $240$  K. Detailed galvano- and thermo-magnetic studies reveal that the enhanced Seebeck coefficient of the  $\text{Bi}_{82}\text{Sb}_{18}/\text{Al}_2\text{O}_3$  nanocomposite samples is originated from more optimal doping level of the samples. In contrast, the presence of the  $\text{Al}_2\text{O}_3$  nanoparticles hardly affects the effective mass or the scattering parameter. Our study suggests the possibility of improving thermoelectric performance of nanocomposites by optimal doping, even for materials wherein the presence of nanostructure yields unfavorable effect on the electrical to thermal conductivity ratio.

## **ACKNOWLEDGMENTS**

The work was supported by Basic Science Research Program through the National Research Foundation of Korea (NRF) funded by the Ministry of Education (2017R1D1A1B03034331), and by Nano·Material Technology Development Program through the NRF funded by Ministry of Science and I CT (2017M3A7B8065589). JPH is supported by the Center for Emergent Materials: an NSF MRSEC under Award DMR-1420451.

## Figure Captions

FIG. 1. (Color online) Calculated thermoelectric figure-of-merit ( $zT$ ) of  $\text{Bi}_{100-x}\text{Sb}_x$  alloys at 300 K from the data on the undoped single crystalline samples in Ref. [5]. The result for the polycrystal was obtained by taking weighted averages of the data along the three crystallographic directions. Symbols indicate calculated data points and lines are added to guide the eye.

FIG. 2. (Color online) Scanning electron microscopy (SEM) pictures for  $\text{Bi}_{82}\text{Sb}_{18}/\text{Al}_2\text{O}_3$  nanocomposite samples with (a, b) 5 vol. % and (c, d) 20 vol. %  $\text{Al}_2\text{O}_3$  nanoparticles. Scale bar is shown on the bottom-right corner of each picture.

FIG. 3. (Color online) Temperature dependence of thermoelectric properties of  $\text{Bi}_{82}\text{Sb}_{18}$  alloy samples. (a) Thermal conductivity ( $\kappa$ ), (b) Electrical resistivity ( $\rho$ ), (c) Seebeck coefficient ( $S$ ), (d) Figure-of-merit ( $zT$ ). The data for the single crystalline sample were calculated by taking a weighted average of the data from Ref. [5] along the three crystallographic directions. Inset in (a) shows the magnetic field dependence of  $\kappa$  normalized by the zero-field value at  $T = 100$  K. Figure legend is included in (c). Symbols are experimental data points and lines are added to guide the eye.

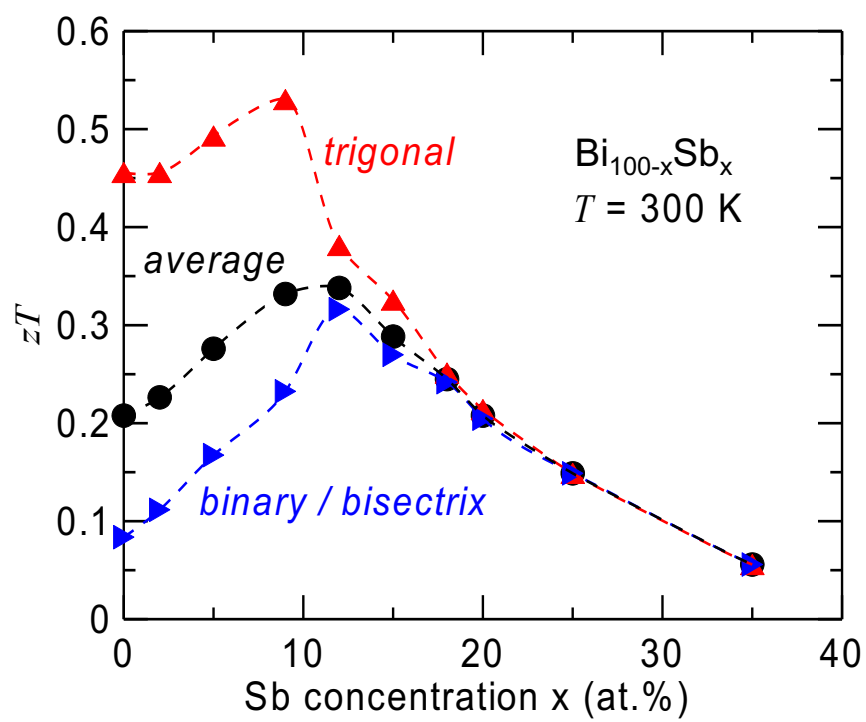
FIG. 4. (Color online) Temperature dependence of (a) carrier concentration ( $n$ ), (b) Hall mobility ( $\mu_H$ ), and Nernst coefficient ( $N$ ) of  $\text{Bi}_{82}\text{Sb}_{18}$  alloy samples. Figure legend is included in (a). (d) Dependence of  $(3/2 + \lambda) \cdot m^*$  on  $\text{Al}_2\text{O}_3$  concentration at  $T = 100$  and 140 K, where  $\lambda$  is the scattering parameter and  $m^*$  is the density-of-state effective mass of electrons. Symbols are experimental data points and lines are added to guide the eye.



FIG. 5. (Color online) Temperature dependence of thermoelectric properties of  $\text{Bi}_{88}\text{Sb}_{12}$  alloy samples. (a) Thermal conductivity ( $\kappa$ ), (b) Electrical resistivity ( $\rho$ ), (c) Seebeck coefficient ( $S$ ), (d) Figure-of-merit ( $zT$ ). The data for the single crystalline sample were calculated by taking a weighted average of the data from Ref. [5] along the three crystallographic directions. Figure legend is included in (c). Symbols are experimental data points and lines are added to guide the eye.

FIG. 6. (Color online) Temperature dependence of (a) carrier concentration ( $n$ ), (b) Hall mobility ( $\mu_H$ ), and Nernst coefficient ( $N$ ) of  $\text{Bi}_{88}\text{Sb}_{12}$  alloy samples. Figure legend is included in (a). (d) Dependence of  $(3/2 + \lambda) \cdot m^*$  on  $\text{Al}_2\text{O}_3$  concentration at  $T = 100$  and  $140$  K, where  $\lambda$  is the scattering parameter and  $m^*$  is the density-of-state effective mass of electrons. Symbols are experimental data points and lines are added to guide the eye.

Figure 1



**Figure 2**

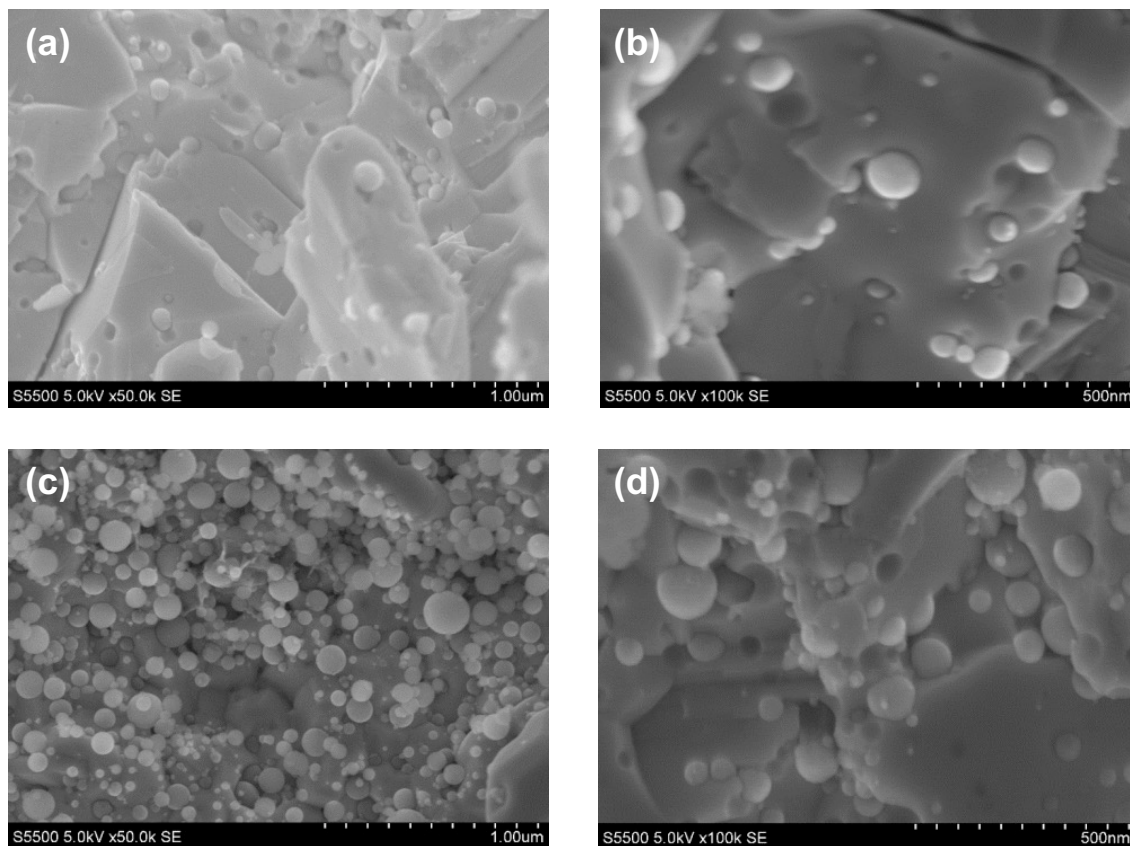


Figure 3

$\text{Bi}_{82}\text{Sb}_{18}$

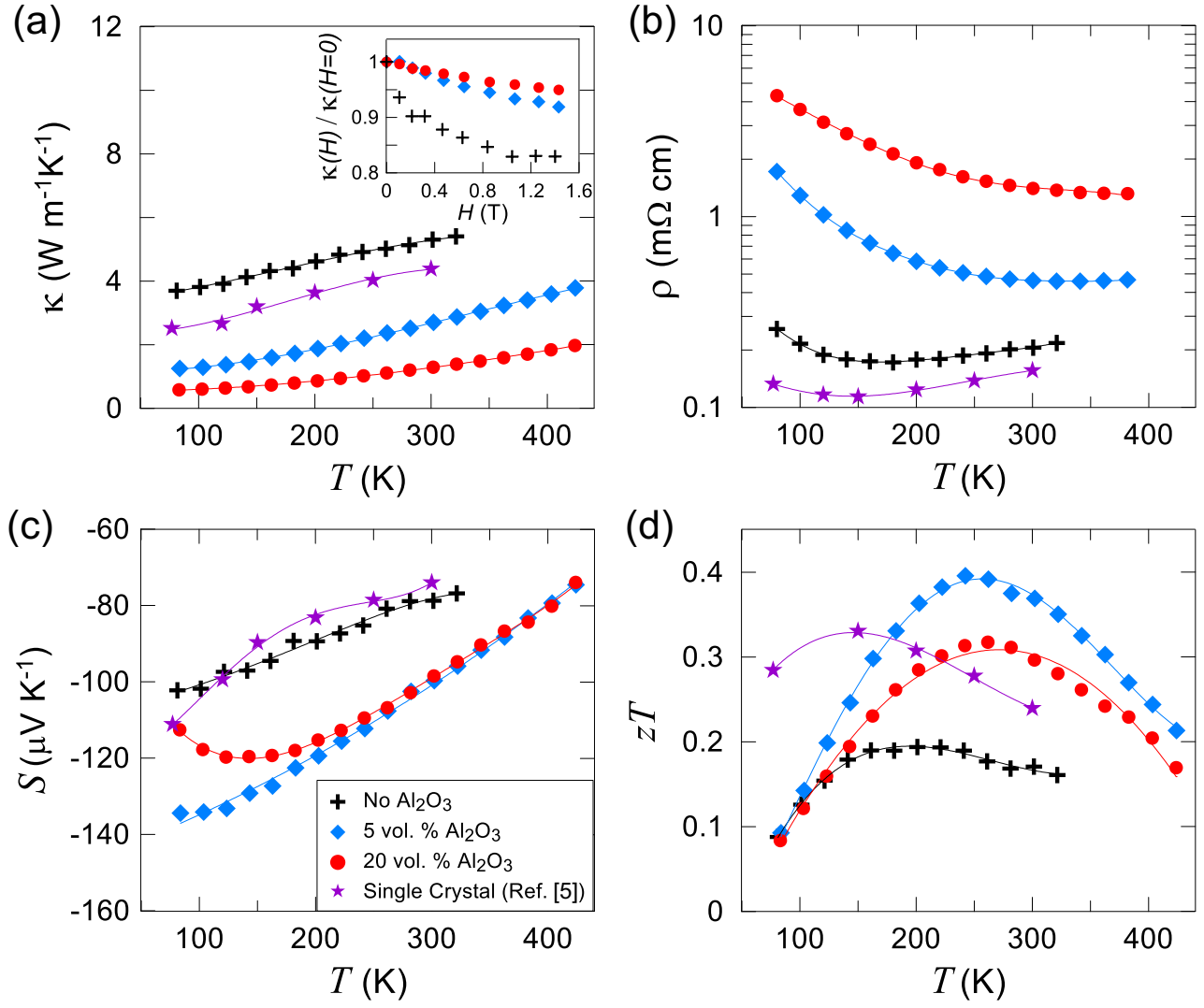


Figure 4

$\text{Bi}_{82}\text{Sb}_{18}$

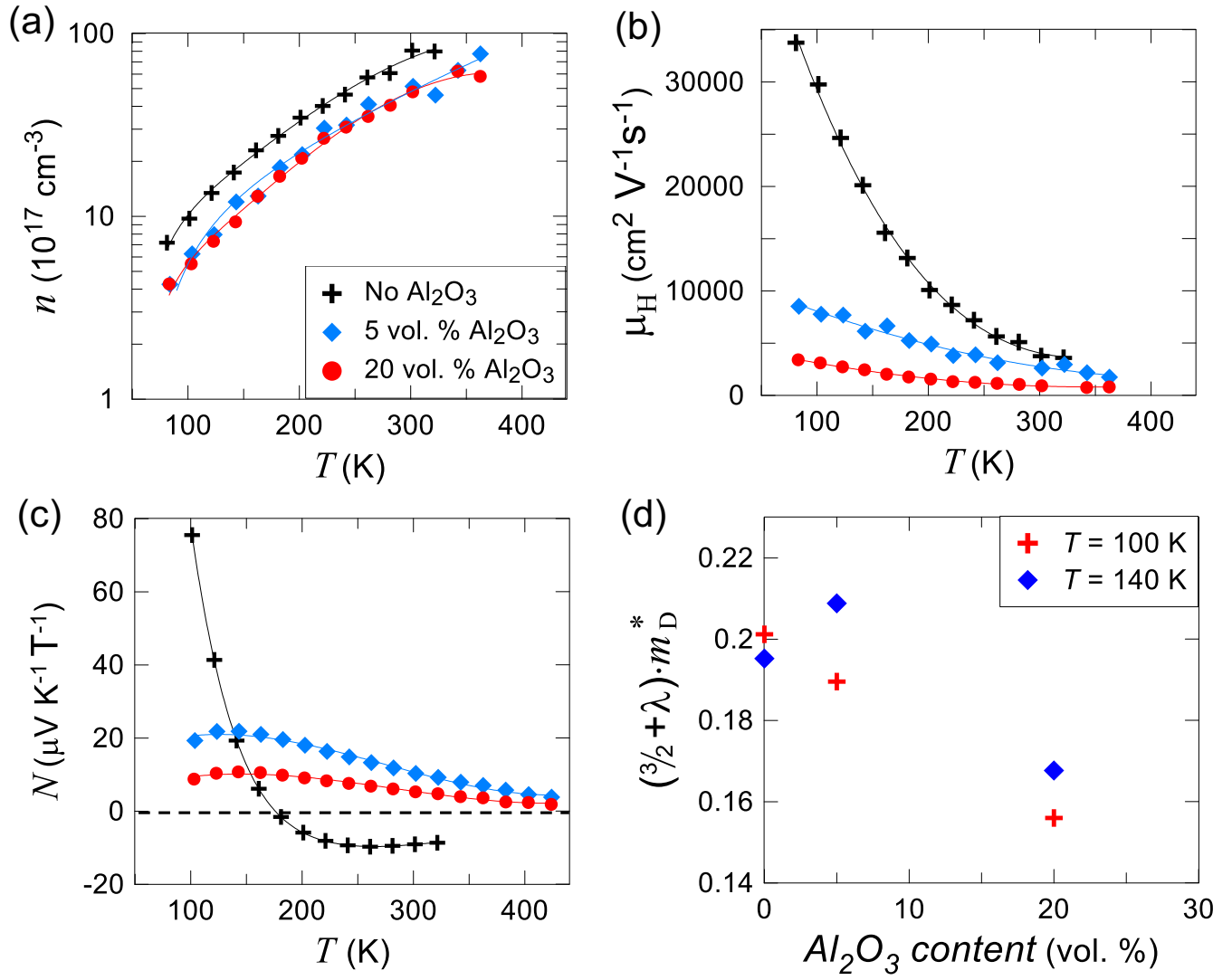


Figure 5

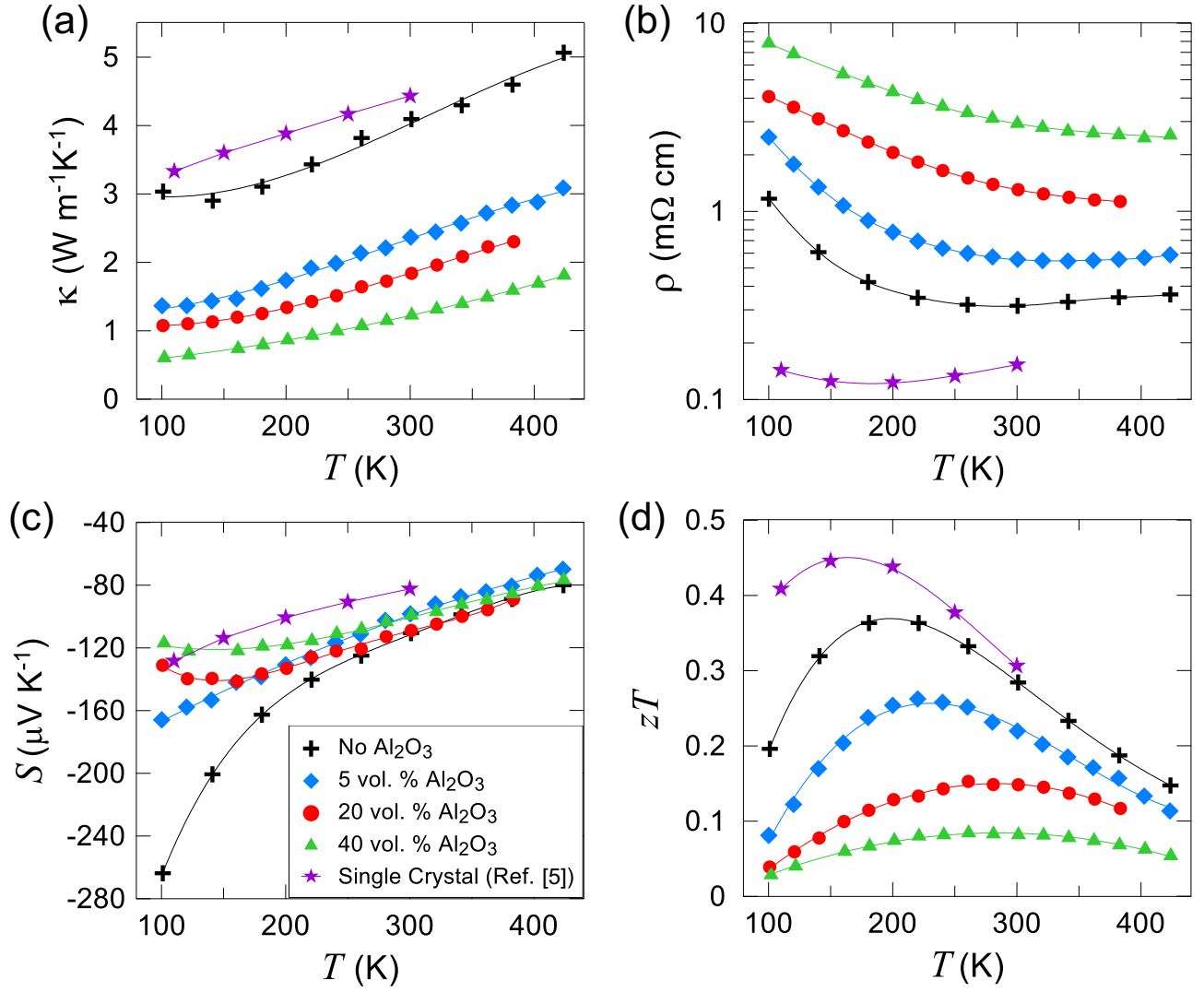
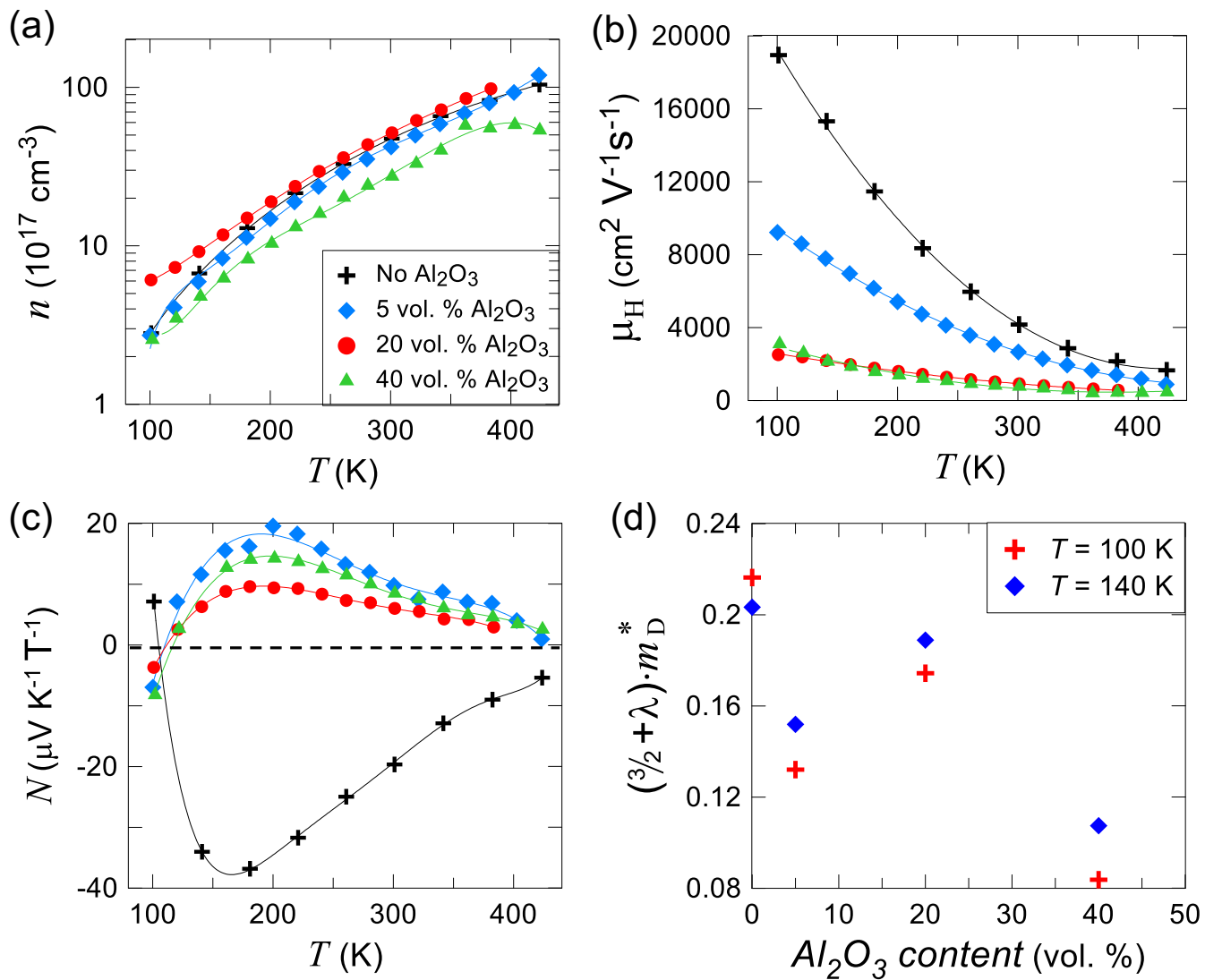


Figure 6

$\text{Bi}_{88}\text{Sb}_{12}$



## References

---

- <sup>1</sup> J. P. Heremans and H. Jin, Proc. SPIE **9765**, 976507 (2016); doi: 10.1117/12.2208541
- <sup>2</sup> C. F. Gallo, B. S. Chandrasekhar, and P. H. Sutter, Transport properties of bismuth single crystals, J. Appl. Phys. **34**, 144 (1963).
- <sup>3</sup> H. Jin, C. M. Jowski, and J. P. Heremans, Enhancement in the figure of merit of p-type  $\text{Bi}_{100-x}\text{Sb}_x$  alloys through multiple valence-band doping, Appl. Phys. Lett. **101**, 053904 (2012).
- <sup>4</sup> J. P. Heremans, R. J. Cava, and N. Samarth, Tetradymites as Thermoelectrics and Topological Insulators, Nature Reviews Materials **2**, 17049 (2017).
- <sup>5</sup> W. M. Yim and A. Amith, Bi-Sb alloys for magneto-thermoelectric and thermomagnetic cooling, Solid-State Electronics **15**, 1141 (1972).
- <sup>6</sup> G. E. Smith and R. Wolfe, Thermoelectric properties of bismuth-antimony alloys, J. Appl. Phys. **33**, 841 (1962).
- <sup>7</sup> P. Jandl and U. Birkholz, Thermogalvanomagnetic properties of Sn-doped  $\text{Bi}_{95}\text{Sb}_5$  and its application for solid state cooling, J. Appl. Phys. **76**, 7351 (1994).
- <sup>8</sup> V. S. Zemskov, A. D. Belaya, U. S. Beluy, and G. N. Kozhemyakin, Growth and investigation of thermoelectric properties of Bi-Sb alloy single crystals, J. Crystal Growth **212**, 161 (2000).
- <sup>9</sup> N. A. Sidorenko and L. D. Ivanova, Bi-Sb solid solutions: Potential materials for high-efficiency thermoelectric cooling to below 180 K, Inorganic Mater. **37**, 331 (2001).
- <sup>10</sup> B. Lenoir, M. Cassart, J.-P. Michenaud, H. Scherrer, and S. Scherrer, Transport properties of Bi-rich Bi-Sb alloys, J. Phys. Chem. Solids **57**, 89 (1996).
- <sup>11</sup> B. Lenoir, A. Dauscher, M. Cassart, Yu. I. Ravich, and H. Scherrer, Effect of antimony content on the thermoelectric figure of merit of  $\text{Bi}_{1-x}\text{Sb}_x$  alloys, J. Phys. Chem. Solids **59**, 129 (1998).



- 
- <sup>12</sup> R. Martin-Lopez, A. Dauscher, H. Scherrer, J. Hejtmanek, H. Kenzari, and B. Lenoir, Thermoelectric properties of mechanically alloyed Bi-Sb alloys, *Appl. Phys. A* **68**, 597 (1999).
- <sup>13</sup> X. Devaux, F. Brochin, R. Martin-Lopez, and H. Scherrer, Study of the microstructure influence on the transport properties of Bi<sub>86.5</sub>Sb<sub>13.5</sub> polycrystalline alloy, *J. Phys. Chem. Solids* **63**, 119 (2002).
- <sup>14</sup> J. P. Heremans, C. M. Thrush, and D. T. Morelli, Thermopower enhancement in lead telluride nanostructures, *Phys. Rev. B* **70**, 115334 (2004).
- <sup>15</sup> B. Poudel, Q. Hao, Y. Ma, Y. Lan, A. Minnich, B. Yu, X. Yan, D. Wang, A. Muto, D. Vashaee, X. Chen, J. Liu, M. S. Dresselhaus, G. Chen, and Z. Ren, High-thermoelectric performance of nanostructured bismuth antimony telluride bulk alloys, *Science* **320**, 634 (2008).
- <sup>16</sup> T. Zhu, C. Fu, H. Xie, Y. Liu, and X. Zhao, High efficiency Half-Heusler thermoelectric materials for energy harvesting, *Adv. Energy Mater.* **5**, 1500588 (2015).
- <sup>17</sup> W. Xie, A. Weidenkaff, X. Tang, Q. Zhang, J. Poon, and T. M. Tritt, Recent advances in nanostructured thermoelectric Half-Heusler compounds, *Nanomaterials* **2**, 379 (2012).
- <sup>18</sup> L. D. Hicks and M. S. Dresselhaus, Effect of quantum-well structures on the thermoelectric figure of merit, *Phys. Rev. B* **47**, 12727 (1993).
- <sup>19</sup> L. D. Hicks and M. S. Dresselhaus, Thermoelectric figure of merit of a one-dimensional conductor, *Phys. Rev. B* **47**, 16631 (1993).
- <sup>20</sup> J. P. Heremans, C. M. Thrush, D. T. Morelli, and M-C. Wu, Thermoelectric power of bismuth nanocomposites, *Phys. Rev. Lett.* **88**, 216801 (2002).
- <sup>21</sup> J. P. Heremans, Low-dimensional thermoelectricity, *Acta Physica Polonica* **108**, 609 (2005).
- <sup>22</sup> J-P. Issi, J. P. Heremans, and M. S. Dresselhaus, Electronic and Lattice Contributions to the Thermal Conductivity of Graphite Intercalation Compounds, *Phys. Rev. B* **27**, 1333 47 (1983).

- 
- <sup>23</sup> C. Uher and H. J. Goldsmid, Separation of the Electronic and Lattice Thermal Conductivities in Bismuth Crystals, *Phys. Stat. Solidi (b)* **65**, 765 (1974).
- <sup>24</sup> J. W. Sharp and H. J. Goldsmid, Boundary scattering of charge carriers and phonons, *Proc. 18<sup>th</sup> Intl. Conf. Thermoelectrics*, 709 (1999).
- <sup>25</sup> E. H. Volckmann, H. J. Goldsmid, and J. Sharp, Observation of the effect of grain size on the lattice thermal conductivity of polycrystalline bismuth antimony, *Proc. 15<sup>th</sup> Intl. Conf. Thermoelectric*, 22 (1996).
- <sup>26</sup> J. W. Sharp, E. H. Volckmann, and H. J. Goldsmid, The thermal conductivity of polycrystalline  $\text{Bi}_{88}\text{Sb}_{12}$ , *Phys. Stat. Sol. (a)* **185**, 257 (2001).
- <sup>27</sup> J. P. Heremans, C. M. Thrush, and D. T. Morelli, Thermopower Enhancement in PbTe with Pb Precipitates, *J. Appl. Phys.* **98**, 063703 (2005).
- <sup>28</sup> Yu. I. Ravich, B. A. Efimova, and I. A. Smirnov, *Semiconducting Lead Chalcogenides* (Plenum, New York, 1970).
- <sup>29</sup> P. Jandl and U. Birkholz, Thermogalvanomagnetic properties of Sn-doped  $\text{Bi}_{95}\text{Sb}_5$  and its application for solid state cooling, *J. Appl. Phys.* **76**, 7351 (1994).
- <sup>30</sup> M. Le Goff and J. P. Heremans, *J. Phys. F: Met. Phys.* **14**, 399 (1984).
- <sup>31</sup> M. P. Vecchi, E. Mendez, and M. S. Dresselhaus, Temperature Dependence of the Band Parameters in Bi and  $\text{Bi}_{1-x}\text{Sb}_x$  Alloys, *Proc. 13<sup>th</sup> Int. Conf. on Physics of Semiconductors*, 459 (1976).